

RESEARCH

Open Access



Cisplatin-loaded metal–phenolic network with photothermal-triggered ROS generation for chemo-photothermal therapy of cancer

Xiaoxiao Chen¹, Lulu Wang⁴, Sijia Liu⁴, Xuezheng Luo^{4*}, Kai Wang^{3*} and Qizhi He^{2*}

*Correspondence:

xuezhengluo2013@163.com;
kaiwangcn2020@sina.com;
qizhihe2013@163.com

¹ Department of Gynecology, Shanghai First Maternity and Infant Hospital, School of Medicine, Tongji University, Shanghai 201204, China

² Department of Pathology, Shanghai Key Laboratory of Maternal Fetal Medicine, Shanghai Institute of Maternal-Fetal Medicine and Gynecologic Oncology, Shanghai First Maternity and Infant Hospital, School of Medicine, Tongji University, Shanghai 201204, China

³ Clinical and Translational Research Center, Shanghai Key Laboratory of Maternal Fetal Medicine, Shanghai Institute of Maternal-Fetal Medicine and Gynecologic Oncology, Shanghai First Maternity and Infant Hospital, School of Medicine, Tongji University, Shanghai 201204, China

⁴ Department of Gynecology, Obstetrics and Gynecology Hospital of Fudan University, Shanghai 200011, China

Abstract

Developing multifunctional composites has received widespread attention for cancer treatment. Herein, a metal–phenolic network (MPN)-based composite loading with chemotherapy agents (TAFP) exhibits high anti-tumor therapeutic efficacy via photothermal therapy (PTT), chemo-dynamic therapy (CDT), and chemotherapy. The nanocomposite was formed by mixing the chemotherapeutic drugs (cisplatin, DDP) into the tannic acid (TA) and Fe³⁺ network (TAFE) to integrate the synergistic effect of PTT, CDT, and chemotherapy. Due to the acidic tumor microenvironment, the active substances could be released with the degradation of the metal–phenolic network, and the released DDP would induce the chemotherapy. More importantly, the released TA under the acidic environment could increase iron bioavailability by converting Fe³⁺ to Fe²⁺, which converts hydrogen peroxide (H₂O₂) to highly toxic hydroxyl radical via the Fenton reaction. Meanwhile, the heat generated from TAFP after near-infrared (NIR) laser irradiation could enhance the therapeutic effect of CDT and chemotherapy. Furthermore, the composite exhibited unique anticancer efficacy in vivo with low toxicity. Collectively, this work may facilitate the development of metal–phenolic network-based photothermal agents for clinic anti-tumor applications.

Keywords: Cancer, Metal–phenolic network, Photothermal therapy, Chemo-dynamic therapy

Introduction

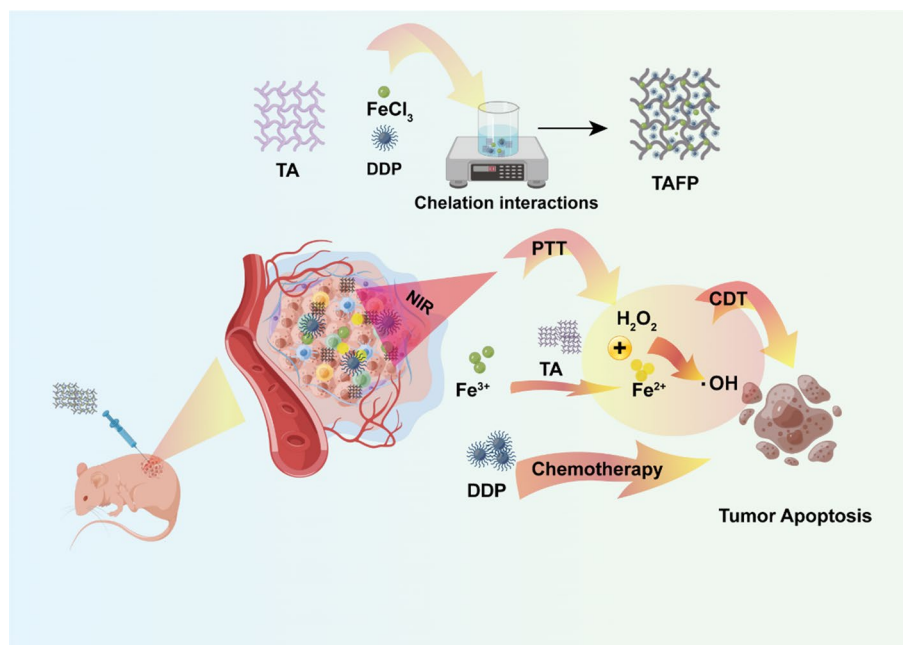
Cancer has become a great social burden for its mortality rate (Siegel et al. 2022). Traditional strategies mainly include surgical excision and chemotherapy of the tumor. For surgical excision, it is very hard to remove all tumor cells by surgery, which often causes postoperative metastases or tumor recurrence. Furthermore, conventional chemotherapy usually causes severe side effects and drug resistance (Marcus et al. 2014; Zahedi et al. 2012). As a result, finding new treatments to improve anti-tumor efficacy is crucial.

The chemotherapy–dynamic therapy (CDT) is a burgeoning treatment strategy in which Fenton reactions generate hydroxyl radicals with high cytotoxicity for inducing apoptosis in cancer cells (Li et al. 2020a, b; Min et al. 2020; He et al. 2021). Hydroxyl



radical is believed to be the most potent and toxic reactive oxygen species (ROS) in biology, causing more harmful oxidative damage to tumor cells (Dong et al. 2019; Li Yang et al. 2020). The majority of the CDT agents are iron-based inorganic nanomaterials, such as iron nanometallic glasses (AFenPs) (Zhang et al. 2016), Fe₃O₄ nanoparticles (Shen et al. 2018), and FePt nanoparticles (Ma et al. 2017). Briefly, iron-based nanomaterials dissolve ferrous ions under the weakly acidic conditions of the tumor microenvironment (TME) and trigger the Fenton reaction to overproduce H₂O₂, generating hydroxyl radical to trigger apoptosis and suppress tumors. Most importantly, this approach is safe for normal tissues, as the Fenton reaction is substantially inhibited under slightly alkaline conditions and in the absence of H₂O₂ in the normal microenvironment (Szatrowski and Nathan 1991). Furthermore, the efficiency of CDT can be enhanced by depleting and reducing species in the TME. Tannin acid (TA) is a representative plant polyphenol that has been approved by the US Food and Drug Administration (FDA) for use in food and medicine (Ejima et al. 2013; Liu et al. 2018). It has been used for surface deposition onto nano-therapeutic platforms by coordinating with metal ions to form metal-TA complexes with pH-sensitive decomposition properties (Dai et al. 2018), which could be used to design the nanocomposites to sense and respond to the endogenous triggers of acidic pH in TME (Liu et al. 2022). TA rapidly reduces Fe III to Fe II, which solves the disadvantage of low catalytic efficiency of the Fenton reaction (Zhang et al. 2018; Zheng et al. 2017). Phototherapy, which utilizes photo agents to absorb near-infrared (NIR) light (650–1350 nm) to induce a therapeutic response, has attracted considerable attention. It not only eliminates tumor cells by hyperthermia but also stimulates systemic immune responses by promoting the release of tumor-associated antigens (TAAs) and tumor-specific antigens (TSAs). Moreover, mild photothermal heating can enhance the uptake of nano drugs by tumor cells and further trigger the release of therapeutic agents, enhancing the anticancer effect through a synergistic manner of PTT and chemotherapy (Chen et al. 2019). Besides, by generating local heat from PTT, the Fenton reaction was further accelerated, resulting in CDT with high efficiency (Nie et al. 2019). Certainly, chemotherapy can also indirectly increase the efficiency of CDT by inhibiting certain specific cell signals to promote cell death (Deng et al. 2019). Compared with monotherapies, such as chemotherapy or immunotherapy, synergistic effects significantly enhanced tumor suppression (Zhou et al. 2021). Therefore, a synergistic therapeutic strategy that significantly boosted tumor suppression is becoming an increasingly important trend in cancer treatment. However, most of the previous research based on two mechanisms presents synergistic cancer therapy, such as PTT/CDT, CDT/chemotherapy, and PTT/chemotherapy (Hu et al. 2021, 2018), and little effort has been devoted to developing a platform for achieving synergistic PTT/CDT/chemotherapy.

In this study, the platform based on metal-phenolic network was successfully developed using a simple one-pot method at room temperature (Scheme 1) and exhibited a superior antitumor effect via PTT/CDT/chemotherapy synergistic strategy. As illustrated in Scheme 1, the resulting composites TAFP exhibited an excellent photothermal effect in killing cancer cells under 808 nm laser irradiation. Meanwhile, the conversion of Fe³⁺ to Fe²⁺ by TA could transfer the mild oxidant H₂O₂ into highly toxic hydroxyl radicals, which induce CDT to kill cancer cells via the Fenton reaction as mentioned above. In addition, the TAFP could generate ROS under NIR laser irradiation, which enhanced



Scheme 1 Scheme illustration of the fabrication process of TAFP composites, and the antitumor procedure of TAFP composites via the PTT/CDT/chemotherapy synergistic effect

the CDT effect. Moreover, the acidic pH microenvironment enabled the release of DDP from the network, which could penetrate deeper into the tumor to enhance the anti-tumor effect. Overall, due to the synergistic effects of PTT/CDT/chemotherapy, the TAFP showed great potential in anti-tumor therapy and represented a simple strategy for designing powerful metal-based composites.

Materials and methods

The main reagents and materials

Tannic acid (TA) and chloride hexahydrate ($\text{FeCl}_3 \cdot 6\text{H}_2\text{O}$) were obtained from Aladdin Reagent Company (Shanghai, China). Cisplatin (DDP), 4',6-diamidino-2-phenylindole (DAPI), Cell Counting Kit-8 (CCK-8), PI/calcein-AM and Reactive Oxygen Species (ROS) Assay Kit were purchased from Beyotime Biotechnology (Shanghai, China). FITC-DDP was purchased from QIYUE biology (Xian, China). An 808 nm NIR laser device (Shanghai Connect Fiber Optics Company) and a near-infrared thermal imaging camera (FLIR™ A325SC camera) were applied for photothermal therapy. SKVO3 cells were purchased from Sangon Biotech Co., Ltd.

Synthesis of TAF_e and TAFP

TAF_e was synthesized via a self-assembly method. Briefly, TA and FeCl_3 were dispersed in deionized water and stirred for 30 min at a molar mass ratio of 1: 4 at room temperature. Then, the mixture were collected by centrifugation and further washed with deionized water several times to remove the excess TA or FeCl_3 . For the synthesis of TAFP or FITC-labeled TAFP, TA, DDP or FITC-DDP and $\text{FeCl}_3 \cdot 6\text{H}_2\text{O}$ were first dispersed in deionized water, respectively, at a molar mass ratio of 1:1:4. The DDP was mainly dispersed in water using ultrasonic dispersion method. Then, the above solutions were

mixed and stirred for 30 min. The final products was washed as described above for further use.

Physicochemical characterization

The morphology of the TAFP complex was characterized by the scanning electron microscopy with the accessory EDS system (SEM, FEI, Nova 450, USA). The morphology and surface chemistry of the TAFP was further performed through Transmission electron microscopy (TEM, FEI, Talos F200S, USA). The diameter distribution and zeta potential of the TAFP were determined via dynamic light scattering measurements (Zetasizer nano, Malvern, UK), and the spectrum of the composites were analyzed via Fourier Transform Infrared Spectroscopy (FTIR, Thermo Scientific Nicolet iS5, USA). The surface chemistry of TAFP was analyzed via X-ray photoelectron spectroscopy (XPS, Thermo ESCALAB 250XI, USA). Ultraviolet–visible (UV–vis) absorption spectra of TAFP was recorded via an UV–vis spectrometer (Thermo Scientific, USA). The degradation of TAFP composites were evaluated by dissolving in PBS with various pH values of 7.4, 6.5, and 5.5 for 24 h to simulate neutral healthy body fluids and acidic TME.

Loading efficiency of DDP by high-performance liquid chromatography (HPLC)

The loading efficiency was performed and analyzed using Agilent HPLC 1260 with Hypersil-ODS2 chromatographic column (250 mm × 4.6 mm, 5 μm). Separation was carried out at 23 °C, and the mobile phase was a mixture of water, methanol and acetonitrile (31:31:38), with a constant flow of 1.6 mL/min. Detection was performed at 254 nm as previous reported (Toro-Córdova et al. 2016). Briefly, 1 mg DDP was added in the mixture (10 mL) and stirred as described in the manuscript. The supernatant was then collected after centrifugation for further detection. Concentrations were calculated from peak areas of standard calibration curves using HPLC software. The loading efficiency was calculated following the equation: $(\text{The amount of drug loaded})/(\text{amount of drug before loading}) \times 100\%$.

In vitro photothermal measurement

To assess the photothermal performance of composites, 100 μL TAFP solutions ultrasonically dispersed in PBS was added into 96 well plate at different concentrations (25, 50, 100, 200, 400 μg/mL), and then treated with 808 nm laser irradiation (1 W/cm², 10 min). Then, 200 μg/mL TAFP solutions was treated with 808 nm NIR for 10 min at different power values (0.5, 1, 1.5, 2 W/cm²). 100 μL PBS as a control group was also treated with 808 nm NIR for 10 min. Then, five circles (200 μg/mL, 1 W/cm²) with lasers on/off were conducted to detect the photothermal stability of TAFP. Thermal imaging cameras (FLIR™ A325SC camera) were applied to collect the temperature changes and data.

Cell culture

The human ovarian cancer cell line of SKVO3 was used to evaluate the anti-tumor efficacy of TAFP, and was originally obtained from Cell Bank of the Chinese Academy of Sciences (Shanghai, China). The SKVO3 cells were grown at 37 °C in RPMI 1640

(HyClone, Logan, UT, USA) containing 10% fetal bovine serum (FBS), 1% penicillin, and 1% streptomycin.

In vitro cytotoxicity assessment

The cytotoxicity of TAFP on SKOV3 was first studied by CCK8 method after incubation with different concentrations of composites. Then, the cytotoxicity of TAFP with or without laser irradiation was further evaluated by CCK8 method. In brief, the SKOV3 cells (1×10^4 per well) dispersed in complete medium were seeded into a 96-well plate to grow overnight. Then, the media were replaced with 100 μ L of medium containing different concentrations of TAFP composites. After co-cultured for 4 h, the cells were treated with or without laser irradiation at a power density of 1 W/cm² for 10 min. The cells were then incubated for another 6 h, followed by removing the medium. Afterward, 110 μ L medium mixed with 10 μ L CCK8 was added to each well and kept at 37 °C. The 450 nm absorbance was measured after 2 h of incubation at 37 °C using a microplate reader (Thermo Fisher, USA). The cell viability was calculated according to the following formula: cell viability = (OD value of test group—OD value of blank group)/(OD value of the untreated group—absorbance of blank group) \times 100%.

For Live/Dead staining, SKOV3 cells (2×10^5) were seeded into a 6-well plate and were cultured overnight for attaching. The cells were then co-cultured with PBS, TAFE (80 μ g/mL), and TAFP (80 μ g/mL) with or without laser irradiation (1 W/cm², 10 min) for 4 h. Calcein-AM/propidium iodide staining reagents was used for identify live and dead cells. Briefly, the media in the 6-well plate were washed with PBS, and co-incubation at 37 °C with 1 ml 0.2 μ M calcein-AM/propidium iodide for 45 min. After washing again with PBS, the cells were observed under a fluorescence microscope (Leica, Germany).

Detection of ROS and in vitro cellular uptake

To evaluate the ROS generation ability of TAFP with or without laser irradiation (1 W/cm², 10 min), DCFH-DA was applied to measure the ROS levels. In brief, a total of 1.0×10^4 SKOV3 cells were seeded into 6-well plates per well and incubated for 24 h overnight. The media were replaced with complete medium with 80 μ g/mL TAFP and co-cultured for 4 h, followed by treating with or without laser irradiation at a power density of 1 W/cm² for 5 min and 10 min, respectively. After incubation for another 4 h, the medium was replaced with DCFH-DA (10 μ M/L) and co-cultured at 37 °C for 10 min. The cells were then washed three times with serum-free culture medium to fully remove DCFH-DA, and observed under a fluorescence microscope. The mean fluorescence intensity of images were calculated using ImageJ software. To detect the cellular uptake activity, the FITC-labeled DDP was applied to prepare the FITC-TAFP as description above. First, the SKOV3 were seeded into a 12-well plate at a density of 1×10^5 cells/well overnight. Then, the medium was replaced with FITC-TAFP composites followed by laser irradiation at 1 W/cm² for 10 min or not. After incubation for 2 and 4 h, the cells were washed with PBS three times and stained with DAPI for 5 min, followed by washing for another 3 times. Then, the cells were observed under the fluorescence microscope.

In vivo antitumor study

SKOV3 cells (3×10^6) were subcutaneously injected into the back of the Balb/c mice to establish the original tumor models. Once the tumor volume reached 60–70 mm³, the mice were randomly divided into 6 groups ($n=4$): (1) PBS (100 μ L), (2) PBS+NIR, (3) TAFE, (4) TAFE+NIR, (5) TAFP, (6) TAFP+NIR. Mice in laser group were then irradiated by an 808 nm laser for 10 min (1 W/cm²) after 1 h of intratumoral injection, and two intensive treatment was conducted on day 3 and day 5. The tumor volume and body weight were recorded every 2 days. The tumor volume was calculated according to the formula: tumor volume = (length \times width²)/2. After 14 days of treatment, the mice were sacrificed, and the tumors were photographed. The main organs and tumors were fixed in 4% formalin for histological analysis. All animal work followed guidelines of the Administration of Affairs Concerning Experimental Animals, and was approved by the Animal Ethical Committee of Tongji University of Science and Technology, China (Approval Number: TJBG11122102).

Statistical analysis

All data were expressed as mean \pm standard deviation (SD). Comparisons among multiple groups were performed using the one-way ANOVA analysis. All the statistical analyses were performed using SPSS statistical software version 25 (IBM Corp, Armonk, NY), and the differences of *** $p < 0.001$, ** $p < 0.01$, * $p < 0.05$ were represented significant difference between groups.

Results

Fabrication and physicochemical characterization of TAFP

As shown in Fig. 1a, the anticancer drug DDP was integrated into the metal–phenolic network (TAFE) via chelation interactions between catechol groups and DDP using a simple one-pot method at room temperature (Zhu and Su 2017). The TEM images and elements mapping showed the morphology of TAFP and the distribution of elements including C, N, Fe, O, Pt (Fig. 1b, c), which indicated the successful synthesis of composites. In addition, the structure and components of the metal–phenolic network loaded with DDP was further characterized by SEM and mapping as shown in Additional file 1: Figs. S1, S2. Meanwhile, a clear Tyndall effect (Fig. 1d) could be observed, indicating the outstanding dispersibility and stability of the composites. The successful integration of DDP could also be proved by the FTIR spectra (Fig. 1e), in which the strong absorption peak of amine at 3285 cm⁻¹ also presented at the TAFP spectra. Meanwhile, the UV–vis spectra showed that the absorption peak near 203 nm were both observed in the spectra of DDP and TAFP (Fig. 1f), which also illustrated the successful loading. As description in the TEM or SEM images, the details of elements could be further detected from the XPS analysis (Fig. 1g), in which Fe³⁺ was evidenced by the peak at 712.5 eV spectrum of Fe 2p, and the Pt 4f spectrum was evidenced by the high-resolution XPS pattern at the peak of 75 eV (Additional file 1: Fig. S3). The EDS of TAFP also confirmed the presence of C, O, Fe, Pt in correspondence with the SEM and TEM results. The mean diameter of TAFP measured by DLS was about 500 nm, as shown in Fig. 1i, which could provide large enough surface

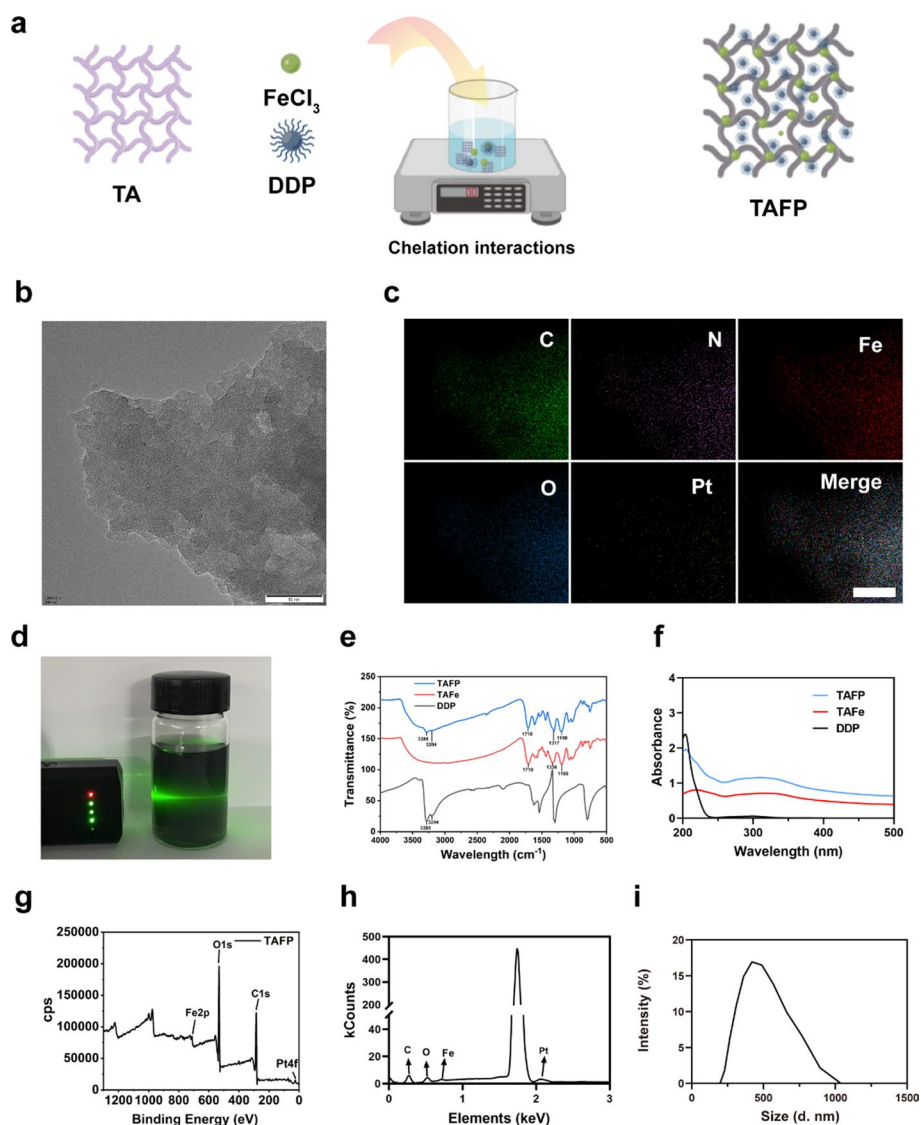


Fig. 1 Characterization of TAFP composites. **a** Fabrication process of TAFP composite. **b** Transmission electron microscopy (TEM) image of TAFP composites. **c** Elements mapping and merged images of TAFP including C, N, Fe, O, Pt elements. Scale bar = 100 nm. **d** Tindal effect of TAFP in deionized water. **e** FTIR spectra of DDP, TAFc, and TAFP. **f** UV-Vis spectra of DDP, TAFc, and TAFP. **g** XPS spectrum of TAFP composites indicating the coexistence of C, O, Fe and Pt elements. **h** EDS of TAFP indicating the coexistence of C, O, Fe and Pt elements. **i** Hydrodynamic size distribution of TAFP

for the absorption of energy from laser irradiation. A zeta potential value other than -30 mV to $+30$ mV is generally considered to have sufficient repulsive force to attain better physical colloidal stability (Park et al. 2020). In addition, HPLC was performed to determine the DDP loading efficiency. As shown in Additional file 1: Fig. S4, the correlation coefficient of the standard curve was 0.9998, which indicated a good linearity. The final concentration of DDP in the supernatant was 45.192 mg/L from the peak area according to the standard curve. As a result, the loading efficiency of DDP was 54.8%, which was enough for chemotherapy in the presence of PTT and CDT. As shown in Additional file 1: Fig. S5, the absolute value of zeta potential for

TAFP was -36.009 , which was greater than 30 mV, indicating its stability in aqueous suspensions. All the above results indicated the successful synthesis of TAFP and its great stability.

In vitro photothermal measurement and degradation

TAFP composite showed an outstanding photothermal-conversion ability by recording the temperature variation. First, the ultraviolet–visible (UV–vis) absorption spectra of deionized water with different concentrations of TAFP in the range of 200 – 900 nm are shown in Fig. 2a, and the standard working curve of absorbance was drawn to determine the excise concentration of TAFP (Fig. 2b). In the photothermal test, a dose-dependent manner of TAFP to absorb infrared light was investigated. As shown in Fig. 2c, d, the temperature gradually increased with the concentration of TAFP increasing from 25 to 400 $\mu\text{g}/\text{mL}$ under the irradiation of NIR laser (808 nm, 1 W/cm^2). The temperature could reach up to 30 $^\circ\text{C}$ and 59.1 $^\circ\text{C}$ at the concentration of 25 $\mu\text{g}/\text{mL}$ and 400 $\mu\text{g}/\text{mL}$, which indicates the dose-dependent photothermal feature of TAFP dispersion. By contrast, the PBS solution displayed no temperature increasing under the same irradiation process, which indirectly indicated the great photothermal-conversion ability of the TAFP composites. Meanwhile, the photothermal property of the TAFP composites were also power-dependent. As shown in Fig. 2e, the final temperature of the TAFP.

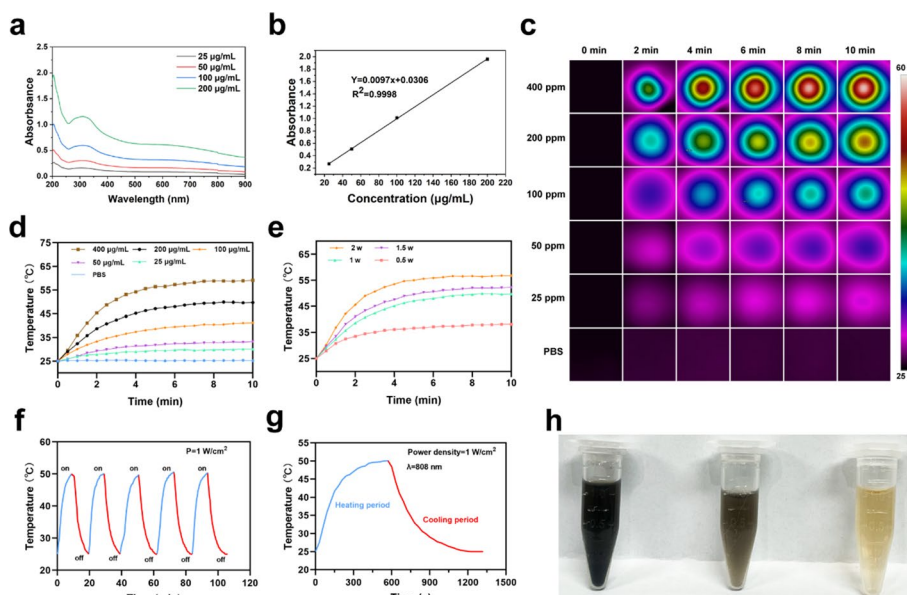


Fig. 2 Photothermal properties of TAFP composites. **a** UV–Vis spectrum of TAFP with different concentrations. **b** Standard curve of TAFP based on the absorbance in UV–vis. **c** Infrared thermal images of PBS and TAFP composites with different concentrations exposed to 808 nm NIR laser irradiation (1 W/cm^2 , 10 min). **d** Temperature variations of TAFP composites at different concentrations under 808 nm NIR laser irradiation (1 W/cm^2 , 10 min). **e** Temperature variations of TAFP composites (200 $\mu\text{g}/\text{mL}$) under the irradiation at various laser power intensities (0.5 , 1.0 , 1.5 , and 2.0 W/cm^2). **f** Temperature variations of TAFP composites exposed to five laser irradiation on/off cycles at a fixed concentration of 200 $\mu\text{g}/\text{mL}$ (1 W/cm^2 , 10 min). **g** Heating/cooling curves of TAFP composites at a fixed concentration of 200 $\mu\text{g}/\text{mL}$ exposed to 808 nm NIR laser irradiation (1 W/cm^2). **h** Digital photos of TAFP composites dispersed in PBS for 24 h with various pH values (from left to right: 7.4 , 6.5 , and 5.5)

Dispersion could be stabilized at 38.2 °C at a weak power density of 0.5 W/cm² and nearly 56.8 °C at a strong power density of 2 W/cm². To further evaluate the photothermal stability of TAFP, the temperature variations of the TAFP dispersion were recorded under the five irradiation cycles at 1 W/cm² for approximately 100 min. After exposure to NIR laser irradiation for 10 min (light on, heating period), the NIR laser was shut down, followed by cooling at room temperature for about 12 min (light off, cooling period). As shown in Fig. 2f, g, the TAFP dispersion displayed excellent photothermal stability without significant reduction in photothermal performance during multiple cycles, indicating its great potential as a powerful photothermal agent based on the metal–phenolic network in tumor therapy (Wang et al. 2018). As a consequence of the degradation of glucose in malignant cells, the production of large amounts of lactic acid would lead to acidic TME (Pérez-Herrero and Fernández-Medarde 2021). For this reason, the state of TAFP composites under different pH environments was evaluated to simulate the degradation in acidic environments. As previously reported, PBS at pH values of 7.4, 6.5, and 5.5 were used to simulate neutral healthy body fluids and acidic TME, respectively (Wu et al. 2021). After incubation at 37 °C for 24 h, the optical photos of three different pH values are shown in Fig. 2h. It was obvious that the TAFP composites degraded dramatically under acidic TME, especially at pH 5.5, while still keeping their original state at pH 7.4. Taken together, these results demonstrated that TAFP could be degraded under the acidic environment, which could provide a pH-responsive system for the treatment of tumor in multiple ways.

In vitro cytotoxicity assessment

Although the TAFP composites showed excellent photothermal properties according to the above results, it was still necessary to evaluate the cytotoxicity of TAFP combined with photothermal therapy at the cellular level. In vitro cytotoxicity assessment, the results showed that TAFP had an excellent therapeutic effect on tumor cells through the combined effect of CDT/PTT/chemotherapy. First, after co-incubating SKOV3 cells with different concentrations of TAFP for 4 h, the cell viability was detected by the method of CCK8. As shown in Fig. 3a, the cytotoxicity of TAFP increases with increasing concentrations, indicating that TAFP had certain cytotoxicity on SKOV3 cells. Then, cells with different TAFP concentrations were treated under NIR irradiation with fixed power density and irradiation time. Figure 3b shows that TAFP was more cytotoxic to tumor cells after laser irradiation and was proportional to the concentration gradient of TAFP. The superb photothermal-conversion performance made TAFP have a more desirable therapeutic effect than the cell viability of the TAFP group was 1.59 times higher than the TAFP + NIR group when the concentration of TAFP was 80 µg/mL. In addition, the live/dead staining results are in agreement with the CCK8 phototoxicity results of TAFP. In Fig. 3c, live/dead staining with calcein AM (green) for live cells and PI (red) for dead was performed to investigate the effects of the combined PTT/CDT/chemotherapy tumor treatment. Cells remained alive in the PBS group with or without irradiation (1 W/cm², 10 min), indicating that irradiation is not intrinsically cytotoxic. After exposure to irradiation, more SKOV3 cells were killed when treated with TAFP or TAFP than those groups without irradiation, verifying that the combination of PTT/CDT displayed better efficacy than monotherapy. In addition, we found that nearly half of the SKOV3

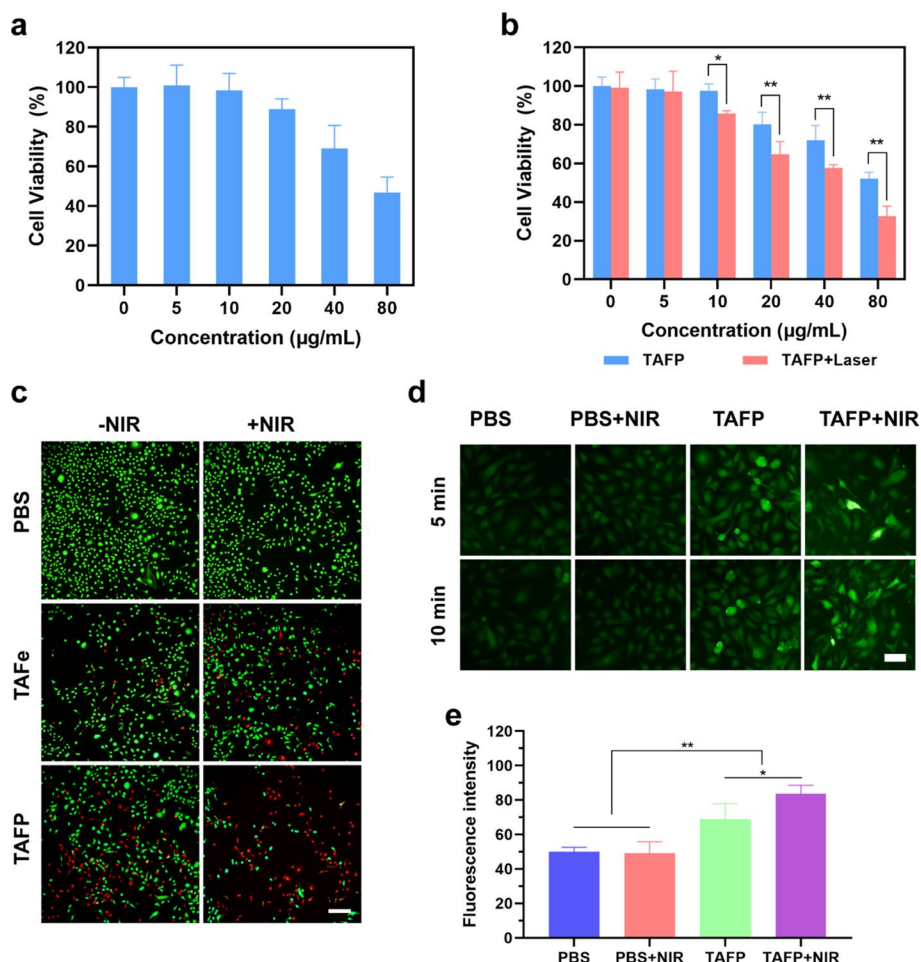


Fig. 3 Cytotoxicity assessments of the TAFP with or without NIR irradiation and detection of ROS generation. **a** Cell viabilities of SKOV3 cells after 24 h co-incubation with TAFP composites at different concentrations. **b** Cell viabilities of SKOV3 cells co-incubated with TAFP composites at different concentrations for 6 h with or without irradiation by 1 W/cm² NIR laser irradiation for 10 min. **c** Digital images of live/dead staining for SKOV3 cells treated with PBS, TAFe and TAFP composites with or without NIR laser irradiation. **d** ROS detection of SKOV3 cells co-incubation with PBS or TAFP with or without NIR laser irradiation. **e** Quantification of fluorescence intensity for SKOV3 cells at 10 min after treated with PBS or TAFP with or without NIR laser irradiation. Scale bar = 100 µm and 200 µm

cells within TAFP without irradiation remained alive, demonstrating that the antitumor effect of CDT/chemotherapy synergistic treatment needs to be further increased. Almost all cells were dead in the TAFP + laser-treated conditions, which suggested that the PTT enhanced the antitumor effect, and confirmed the combination of PTT/CDT/chemotherapy has the best efficacy.

Detection of ROS and the uptake of TAFP by SKOV3

As described above, iron ions released by TAFP bind to H₂O₂ in tumor cells, producing highly toxic hydroxyl radicals through the Fenton reaction and triggering tumor cell apoptosis. Therefore, we examined ROS generation by TAFP in SKOV3 cells using the ROS indicator DCFH-DA. Figure 3d shows that ROS was not produced in PBS/

PBS + laser-treated SKOV3 cells, but the cells treated with TAFP generate a little ROS. After being treated with TAFP + Laser, the generation of ROS significantly increased (Fig. 3e). These phenomena suggested that TAFP could stimulate ROS generation, which could be enhanced under laser irradiation. The uptake of TAFP by SKOV3 cells was also evaluated by fluorescence microscopy after 2 or 4 h of incubation with FITC-labeled TAFP (Additional file 1: Fig. S6). It was further verified that intracellular uptake increased with the prolonged incubation time through the increase in Pt fluorescence originating from TAFP. After exposure to irradiation, the uptake of TAFP was significantly enhanced, which indicated that PTT could promote the uptake of TAFP by tumor cells. These results above suggested that the combination of PTT/CDT/chemotherapy led to preferable anticancer effects.

Photothermal imaging in vivo and anti-tumor efficacy

Encouraged by the excellent photothermal properties and cytotoxicity of the TAFP composites demonstrated by the above experiments, we further evaluated the photothermal imaging and antitumor effects of the TAFP composites in the subcutaneous cancer models in vivo. SKOV3 cells were subcutaneously injected into the back of the mice to establish the original tumor models. Mice in the NIR group was irradiated by an 808-nm laser for 10 min (1 W/cm^2) after 1 h of injection, and another two photothermal treatments on day 3 and day 5 were also conducted. The whole process is displayed in Fig. 4a. As shown in Fig. 4b, the temperature variation in the tumor sites was recorded by thermal imaging. In the TAFE + NIR group and TAFP + NIR group, the final temperature could reach up to about $50 \text{ }^\circ\text{C}$, while only $33.4 \text{ }^\circ\text{C}$ in the PBS + NIR group. Previous studies demonstrated that photothermal could induce cell death through necrosis via high laser intensity ($> 1 \text{ W/cm}^2$) (Melamed et al. 2015; Ng et al. 2016). In brief, the photothermal induces the broken of the cell membrane, which releases the intracellular contents was released, which brings the rapid death of cancer cells without receiving potential resistance to PTT. During 2 weeks, the body weight in each group was recorded. As shown in Fig. 4d, there was no significant difference in body weight, which indicated the negligible systemic toxicity of TAFE or TAFP composites.

In 2 weeks, the tumor volume was recorded every 2 days, and the results showed a significant difference between the group of NIR and without NIR. As shown in Fig. 5a, b, the tumor growth was not inhibited by PBS and PBS + NIR, while greatly suppressed in other groups. In addition, the TAFP group could inhibit tumor growth better than the TAFE group, which indicated the chemotherapy effect via the released DDP. After receiving the treatment of NIR Laser, the tumor volume was further shrunk in the TAFE + NIR group and TAFP + NIR group. Furthermore, the tumor volume showed a significant difference on day 14 between the TAFE + NIR group and the TAFP + NIR group. These results demonstrated that the strategy of PTT/CDT/chemotherapy was an effective method in the synergistic inhibition of tumor. To further confirm the prominent tumor inhibition efficacy of TAFP + NIR via PTT/CDT/chemotherapy, immunohistochemical staining including hematoxylin and eosin (H&E), Ki-67, and terminal deoxynucleotidyl transferase (TUNEL) staining was performed. The H&E and Ki-67 images showed corresponding results as description above.

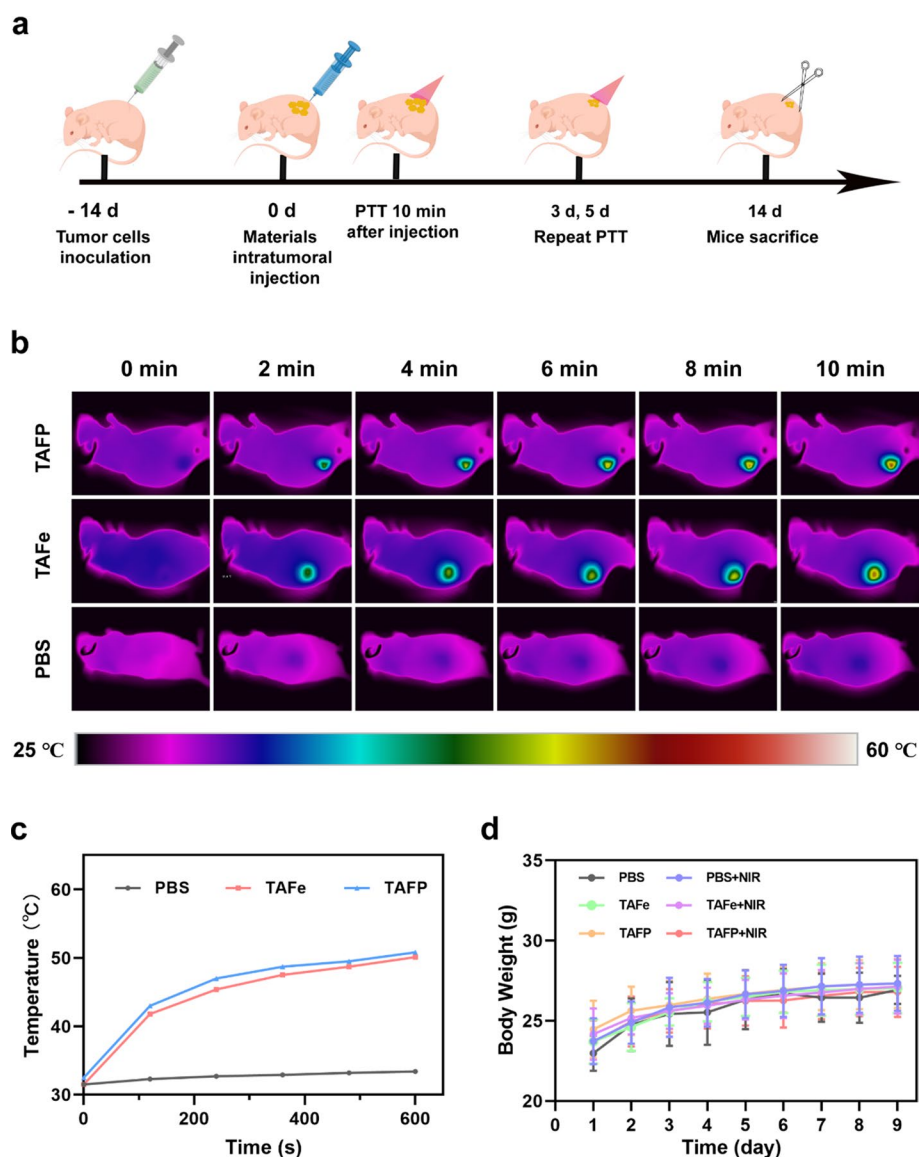


Fig. 4 In vivo photothermal imaging and variations of weight. **a** Schematic illustration of the animal experimental process. **b** Corresponding thermal image of the tumor site injected with PBS, TAFe and TAFP under 808 nm NIR laser irradiation (1 W/cm^2 , 10 min). **c** Temperature variations at the tumor site exposed to 808 nm NIR laser irradiation (1 W/cm^2 , 10 min). **d** Body weight variations of mice during 2 weeks

Especially in TAFP + NIR group, the fewest tumor cells and Ki-67 positive cells were observed in the H&E and Ki-67 images, as shown in Fig. 5c, d. Besides, 808 nm laser greatly induced the apoptosis of the tumor cells, especially in the TAFP + NIR group as shown in Additional file 1: Fig. S7. Moreover, the histocompatibility was evaluated via H&E staining of heart, liver, spleen, lung, and kidneys (Fig. 6), and no toxicity in vivo was observed in these major organs. All the above results suggest that the TAFP composites with laser irradiation could achieve the best therapeutic effect via the PTT/CDT/chemotherapy synergistic treatment without causing noticeable toxicity in vivo, indicating its great potential for application in anticancer treatment.

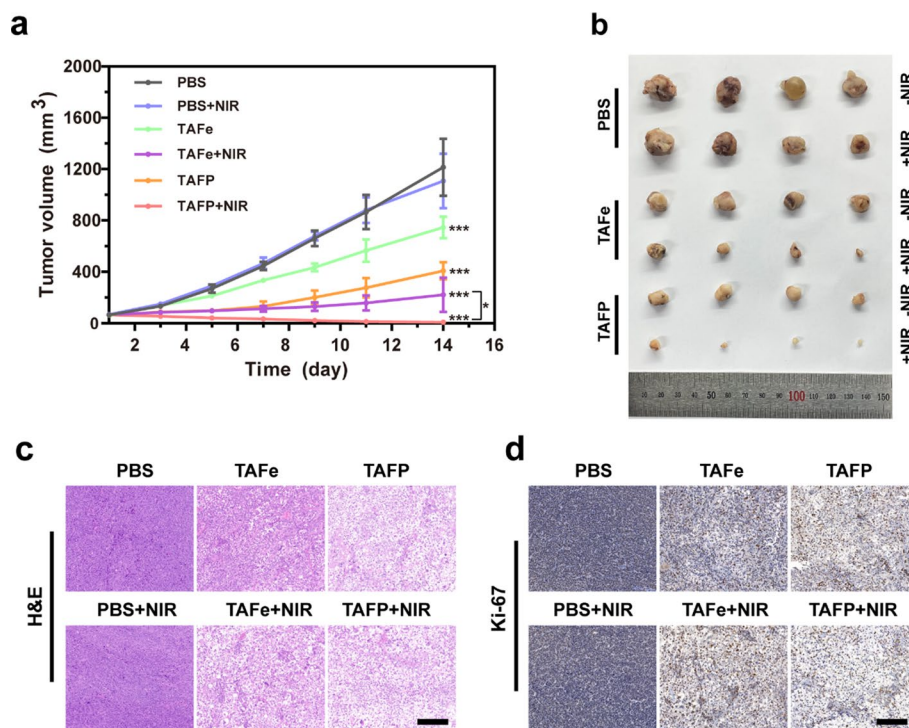


Fig. 5 Antitumor efficacy of synergistic PTT/CDT/chemotherapy. **a** Tumor growth curves of tumors from different groups. **b** Images of the tumor on day 14 after section. **c** H&E staining of tumors after the 14 day treatment; scale bar = 200 μ m. **d** Ki-67 staining of tumors after the 14 day treatment. Scale bar = 200 μ m. (* p < 0.05, *** p < 0.001)

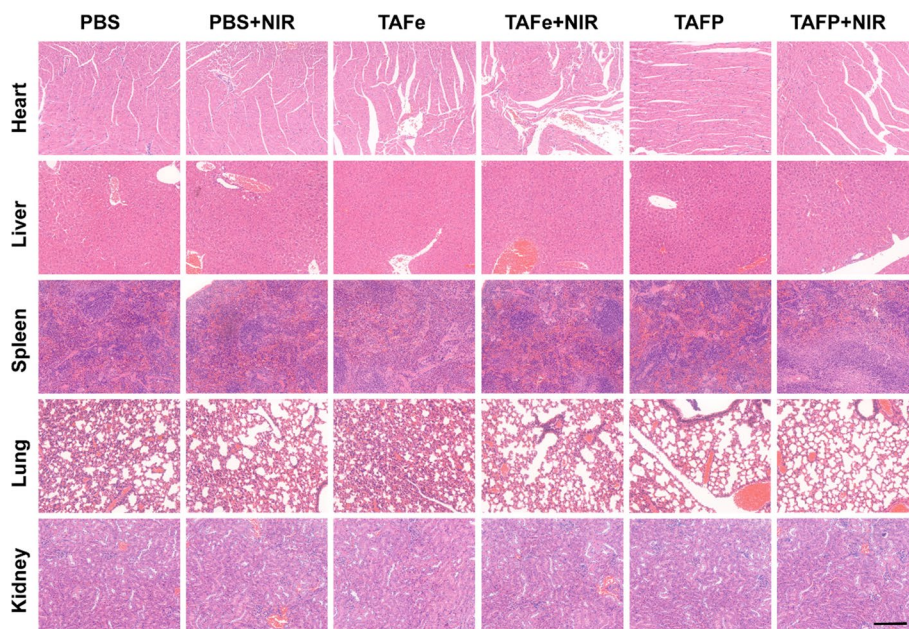


Fig. 6 Pathological sections of the heart, liver, spleen, lung and kidney stained with H&E for biosafety assessment of above groups in vivo. Scale bar = 200 μ m

Discussion

In this study, the TAFP composites exhibited great photothermal-conversion ability and stability as mentioned above. In vitro experiments, it displayed greater cell cytotoxicity under NIR light at 808 nm compared to other groups without NIR light irradiation, which mainly due to the PTT-enhanced CDT/chemotherapy. Meanwhile, a significant tumor reduction and necrosis was observed in the TAFP + NIR group, as shown in Fig. 5. The targeted, local delivery of TAFP via intratumoral injection may reduce the potential for systemic toxicity (Sheth et al. 2020). In addition, the low concentration of chemotherapeutic drug could penetrate deeper into the tumor to enhance the antitumor effect without inducing toxicity in vivo. Therefore, we have demonstrated the great potential of TAFP in cancer treatment in vitro and in vivo.

In clinical, chemotherapeutic drugs including DDP were selected as the first-line chemotherapeutics. However, chemotherapy often induces various side effects, such as nausea-vomiting, nephrotoxicity, and so on (Zhu et al. 2020). As a minimally invasive therapy, photothermal therapy could transduce NIR light into heat to kill tumor cells and has aroused widespread interest (Sheng et al. 2014). In addition, the temperature rise in the tumor site can accelerate the production of ROS to improve the treatment effect via a synergism of CDT/PTT (Li et al. 2017). Many studies utilized photothermal materials to carry chemotherapeutic drugs to realize the synergic antitumor effect and reduce side effects in bimodal methods, such as CDT/chemotherapy, and PTT/chemotherapy (Zhang et al. 2019; Wang et al. 2019). To achieve synergistic PTT/CDT/Chemotherapy in a single platform, we created a metal–phenolic platform to load DDP, which displayed a great synergistic effect on tumor inhabitation as expected. In the current study, the photoresponsiveness of TAFP was mainly attributed to the absorption of light through coordination complexes formed between TA and Fe, and the excellent photothermal-conversion efficiency of TAFE has been approved by researchers (Shim et al. 2020). As a result, we could take full advantage of the TAFP complex to kill tumor cells via synergistic effect at a low concentration of chemotherapeutic drugs, which was important for improving the efficacy of chemotherapy and reducing the side effects.

Conclusions

In summary, a metal–phenolic-based platform loaded with DDP for antitumor via PTT/CDT/chemotherapy synergistic therapy was developed. After intratumorally injected, the tumor growth was greatly suppressed without systemic toxicity under the 808 nm laser irradiation. The TAFP composite in vivo could be degraded and exhibited a synergistic effect in antitumor treatment under mild acidic TME. The released Fe^{3+} could be reduced to Fe^{2+} with the help of TA, which would generate highly toxic hydroxyl radicals via the Fenton reaction. Besides, the 808 laser irradiation could promote the production of ROS to induce the PTT-enhanced CDT. Meanwhile, the DDP could also kill tumor cells via chemotherapy. Overall, TAFP-mediated synergistic therapy could greatly suppress tumor growth without systemic toxicity in vivo, which exhibits broad application prospects in anticancer treatment.

Abbreviations

MPN	Metal–phenolic network
PTT	Photothermal therapy

CDT	Chemo-dynamic therapy
DDP	Cisplatin
ROS	Reactive oxygen species
TAF _e	Tannic acid and Fe ³⁺ network
TME	Tumor microenvironment
DAPI	4',6-Diamidino-2-phenylindole
CCK-8	Cell Counting Kit-8
NIR	Near-infrared
TEM	Transmission electron microscopy
FTIR	Fourier transform infrared spectrum
DLS	Dynamic light scattering
PBS	Phosphate buffered saline
HPLC	High-performance liquid chromatography

Supplementary Information

The online version contains supplementary material available at <https://doi.org/10.1186/s12645-022-00149-4>.

Additional file 1: Figure S1. SEM image of TAFP. **Figure S2.** Elements mapping of TAFP including C, N, O, Pt elements. **Figure S3.** XPS spectrum of Pt 4f in TAFP indicating the existence of Pt element. **Figure S4.** Standard curve of DDP determined by HPLC at 254 nm. **Figure S5.** Zeta potential of TAFP dispersed in DI water. **Figure S6.** Fluorescence images of the uptake of TAFP by SKOV3 cells after co-incubation with TAFP for 2 h and 4 h with or without NIR laser irradiation (10 min, 1 W/cm²). Scale bar = 100 μm. **Figure S7.** TUNEL staining of tumors from each groups after a 14 day treatment. Scale bar = 100 μm.

Acknowledgements

Not applicable.

Author contributions

XC: conceptualization, methodology, investigation, data curation, writing—original draft. LW: formal analysis, methodology, investigation. SL: methodology, validation, investigation. XL: methodology, validation, investigation, resources, project administration, funding acquisition. KW: methodology, validation, investigation, resources, project administration. QH: investigation, resources, project administration. All authors read and approved the final manuscript.

Funding

This research was supported by the Shanghai Natural Science Foundation (No. 18ZR1405300 to Xuezhen Luo).

Availability of data and materials

All data generated or analyzed during this study are included in this published article.

Declarations

Ethics approval and consent to participate

All animal work followed guidelines of the Administration of Affairs Concerning Experimental Animals, and was approved by the Animal Ethical Committee of Tongji University of Science and Technology, China.

Consent for publication

All authors consent for publication.

Competing interests

The authors declared no conflicts of interest.

Received: 23 October 2022 Accepted: 28 November 2022

Published online: 05 December 2022

References

- Chen Q, Luo Y, Du W et al (2019) Clearable theranostic platform with a pH-independent chemodynamic therapy enhancement strategy for synergetic photothermal tumor therapy. *ACS Appl Mater Interfaces* 11:18133–18144
- Dai Y, Yang Z, Cheng S et al (2018) Toxic reactive oxygen species enhanced synergistic combination therapy by self-assembled metal-phenolic network nanoparticles. *Adv Mater*. <https://doi.org/10.1002/adma.201704877>
- Deng X, Liang S, Cai X et al (2019) Yolk-shell structured au nanostar@metal-organic framework for synergistic chemophotothermal therapy in the second near-infrared window. *Nano Lett* 19:6772–6780
- Dong S, Xu J, Jia T et al (2019) Upconversion-mediated ZnFe(2)O(4) nanoplatfor for NIR-enhanced chemodynamic and photodynamic therapy. *Chem Sci* 10:4259–4271
- Ejima H, Richardson JJ, Liang K et al (2013) One-step assembly of coordination complexes for versatile film and particle engineering. *Science* 341:154–157
- He T, Yuan Y, Jiang C et al (2021) Light-triggered transformable ferrous ion delivery system for photothermal primed chemodynamic therapy. *Angew Chem Int Ed Engl* 60:6047–6054

- Hu D, Chen L, Qu Y et al (2018) Oxygen-generating hybrid polymeric nanoparticles with encapsulated doxorubicin and chlorin e6 for trimodal imaging-guided combined chemo-photodynamic therapy. *Theranostics* 8:1558–1574
- Hu T, Yan L, Wang Z et al (2021) A pH-responsive ultrathin Cu-based nanoplatform for specific photothermal and chemodynamic synergistic therapy. *Chem Sci* 12:2594–2603
- Li B, Sun Q, Zhang Y et al (2017) Functionalized porous aromatic framework for efficient uranium adsorption from aqueous solutions. *ACS Appl Mater Interfaces* 9:12511–12517
- Li L, Yang Z, Fan W et al (2020a) In situ polymerized hollow mesoporous organosilica biocatalysis nanoreactor for enhancing ros-mediated anticancer therapy. *Adv Funct Mater*. <https://doi.org/10.1002/adfm.201907716>
- Li Y, Zhao P, Gong T et al (2020b) Redox dyshomeostasis strategy for hypoxic tumor therapy based on DNAzyme-loaded electrophilic ZIFs. *Angew Chem Int Ed Engl* 59:22537–22543
- Liu T, Zhang M, Liu W et al (2018) Metal ion/tannic acid assembly as a versatile photothermal platform in engineering multimodal nanotheranostics for advanced applications. *ACS Nano* 12:3917–3927
- Liu J, He S, Luo Y et al (2022) Tumor-microenvironment-activatable polymer nano-immunomodulator for precision cancer photoimmunotherapy. *Adv Mater* 34:2106654
- Ma P, a, Xiao H, Yu C, et al (2017) Enhanced cisplatin chemotherapy by iron oxide nanocarrier-mediated generation of highly toxic reactive oxygen species. *Nano Lett* 17:928–937
- Marcus CS, Maxwell GL, Darcy KM et al (2014) Current approaches and challenges in managing and monitoring treatment response in ovarian cancer. *J Cancer* 5:25–30
- Melamed JR, Edelstein RS, Day ES (2015) Elucidating the fundamental mechanisms of cell death triggered by photothermal therapy. *ACS Nano* 9:6–11
- Min H, Qi Y, Zhang Y et al (2020) A graphdiyne oxide-based iron sponge with photothermally enhanced tumor-specific fenton chemistry. *Adv Mater* 32:e2000038
- Ng KK, Weersink RA, Lim L et al (2016) Controlling spatial heat and light distribution by using photothermal enhancing auto-regulated liposomes (PEARLs). *Angew Chem Int Ed Engl* 55:10003–10007
- Nie X, Xia L, Wang HL et al (2019) Photothermal therapy nanomaterials boosting transformation of Fe(III) into Fe(II) in tumor cells for highly improving chemodynamic therapy. *ACS Appl Mater Interfaces* 11:31735–31742
- Park JY, Chu GE, Park S et al (2020) Therapeutic efficacy of curcumin enhanced by microscale discoidal polymeric particles in a murine asthma model. *Pharmaceutics*. <https://doi.org/10.3390/pharmaceutics12080739>
- Pérez-Herrero E, Fernández-Medarde A (2021) The reversed intra- and extracellular pH in tumors as a unified strategy to chemotherapeutic delivery using targeted nanocarriers. *Acta Pharm Sin B* 11:2243–2264
- Shen Z, Liu T, Li Y et al (2018) Fenton-reaction-acceleratable magnetic nanoparticles for ferroptosis therapy of orthotopic brain tumors. *ACS Nano* 12:11355–11365
- Sheng Z, Hu D, Zheng M et al (2014) Smart human serum albumin-indocyanine green nanoparticles generated by programmed assembly for dual-modal imaging-guided cancer synergistic phototherapy. *ACS Nano* 8:12310–12322
- Sheth RA, Wen X, Li J et al (2020) Doxorubicin-loaded hollow gold nanospheres for dual photothermal ablation and chemoembolization therapy. *Cancer Nanotechnol* 11:6
- Shim G, Ko S, Park JY et al (2020) Tannic acid-functionalized boron nitride nanosheets for theranostics. *J Control Release* 327:616–626
- Siegel RL, Miller KD, Fuchs HE et al (2022) Cancer statistics, 2022. *CA Cancer J Clin* 72:7–33
- Szatrowski TP, Nathan CF (1991) Production of large amounts of hydrogen peroxide by human tumor cells. *Cancer Res* 51:794–798
- Toro-Córdova A, Ledezma-Gallegos F, Mondragon-Fuentes L et al (2016) Determination of liposomal cisplatin by high-performance liquid chromatography and its application in pharmacokinetic studies. *J Chromatogr Sci* 54:1016–1021
- Wang C, Liu H, Lin X et al (2018) A single lateral rectus abdominis approach for the surgical treatment of complicated acetabular fractures: a clinical evaluation study of 59 patients. *Med Sci Monit* 24:7285–7294
- Wang S, Wang Z, Yu G et al (2019) Tumor-specific drug release and reactive oxygen species generation for cancer chemo/chemodynamic combination therapy. *Adv Sci* 6:1801986
- Wu W, Pu Y, Shi J (2021) Dual size/charge-switchable nanocatalytic medicine for deep tumor therapy. *Adv Sci* 8:2002816
- Zahedi P, Yoganathan R, Piquette-Miller M et al (2012) Recent advances in drug delivery strategies for treatment of ovarian cancer. *Expert Opin Drug Deliv* 9:567–583
- Zhang C, Bu W, Ni D et al (2016) Synthesis of iron nanometallic glasses and their application in cancer therapy by a localized fenton reaction. *Angew Chem Int Ed Engl* 55:2101–2106
- Zhang L, Wan SS, Li CX et al (2018) An adenosine triphosphate-responsive autocatalytic fenton nanoparticle for tumor ablation with self-supplied H₂O₂ and acceleration of Fe(III)/Fe(II) conversion. *Nano Lett* 18:7609–7618
- Zhang C, Zhang D, Liu J et al (2019) Functionalized mos(2)-erlotinib produces hyperthermia under NIR. *J Nanobiotechnology* 17:76
- Zheng DW, Lei Q, Zhu JY et al (2017) Switching apoptosis to ferroptosis: metal-organic network for high-efficiency anti-cancer therapy. *Nano Lett* 17:284–291
- Zhou T, Peng J, Hao Y et al (2021) The construction of a lymphoma cell-based, DC-targeted vaccine, and its application in lymphoma prevention and cure. *Bioact Mater* 6:697–711
- Zhu Z, Su M (2017) Polydopamine nanoparticles for combined chemo- and photothermal cancer therapy. *Nanomaterials*. <https://doi.org/10.3390/nano7070160>
- Zhu C, Luo L, Jiang X et al (2020) Selective intratumoral drug release and simultaneous inhibition of oxidative stress by a highly reductive nanosystem and its application as an anti-tumor agent. *Theranostics* 10:1166–1180

Publisher's Note

Springer Nature remains neutral with regard to jurisdictional claims in published maps and institutional affiliations.